ACCOUNTS of chemical research

Article

pubs.acs.org/accounts

Density Functional Theory Based Study of Molecular Interactions, Recognition, Engineering, and Quantum Transport in π Molecular Systems

Yeonchoo Cho,[†,∥] Woo Jong Cho,[‡,∥] Il Seung Youn,[†,‡] Geunsik Lee,[‡] N. Jiten Singh,[†] and Kwang S. Kim*[,‡]

[†]Center for Superfunctional Materials, Department of Chemistry, Pohang University of Science and Technology, Pohang 790-784, Korea

[‡]Department of Chemistry, Ulsan National Institute of Science and Technology (UNIST), Ulsan 689-798, Korea

CONSPECTUS: In chemical and biological systems, various interactions that govern the chemical and physical properties of molecules, assembling phenomena, and electronic transport properties compete and control the microscopic structure of materials. The well-controlled manipulation of each component can allow researchers to design receptors or sensors, new molecular architectures, structures with novel morphology, and functional molecules or devices. In this Account, we describe the structures and electronic and spintronic properties of π-molecular systems that are important for controlling the architecture of a variety of carbon-based systems. Although DFT is an important tool for describing molecular interactions, the inability of DFT to accurately represent dispersion interactions has made it difficult to properly describe π-interactions. However, the recently developed dispersion corrections for DFT have allowed us to include these dispersion interactions cost-effectively.

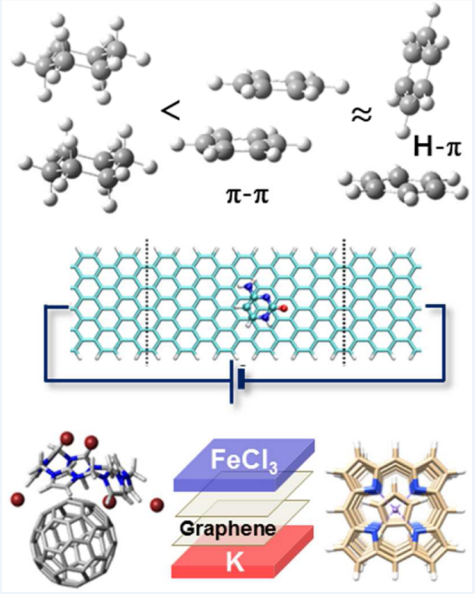

We have investigated noncovalent interactions of various π-systems including aromatic−π, aliphatic−π, and non-π systems based on dispersion-corrected DFT (DFT-D). In addition, we have addressed the validity of DFT-D compared with the complete basis set (CBS) limit values of coupled cluster theory with single, double, and perturbative triple excitations [CCSD(T)] and Møller−Plesset second order perturbation theory (MP2). The DFT-D methods are still unable to predict the correct ordering in binding energies within the benzene dimer and the cyclohexane dimer. Nevertheless, the overall DFT-D predicted binding energies are in reasonable agreement with the CCSD(T) results. In most cases, results using the B97-D3 method closely reproduce the CCSD(T) results with the optimized energy-fitting parameters. On the other hand, vdW-DF2 and PBE0-TS methods estimate the dispersion energies from the calculated electron density. In these approximations, the interaction energies around the equilibrium point are reasonably close to the CCSD(T) results but sometimes slightly deviate from them because interaction energies were not particularly optimized with parameters. Nevertheless, because the electron cloud deforms when neighboring atoms/ions induce an electric field, both vdW-DF2 and PBE0-TS seem to properly reproduce the resulting change of dispersion interaction. Thus, improvements are needed in both vdW-DF2 and PBE0-TS to better describe the interaction energies, while the B97-D3 method could benefit from the incorporation of polarization-driven energy changes that show highly anisotropic behavior.

Although the current DFT-D methods need further improvement, DFT-D is very useful for computer-aided molecular design. We have used these newly developed DFT-D methods to calculate the interactions between graphene and DNA nucleobases. Using DFT-D, we describe the design of molecular receptors of π-systems, graphene based electronic devices, metalloporphyrin half-metal based spintronic devices as graphene nanoribbon (GNR) analogs, and graphene based molecular electronic devices for DNA sequencing. DFT-D has also helped us understand quantum phenomena in materials and devices of π-systems including graphene.

INTRODUCTION

The most basic issue in nanochemistry is how to engineer molecular systems toward interesting properties of materials. Therefore, accurate analysis of molecular interactions is important because their cooperation and competition govern

Special Issue: DFT Elucidation of Materials Properties

Received: December 31, 2013
Published: October 22, 2014

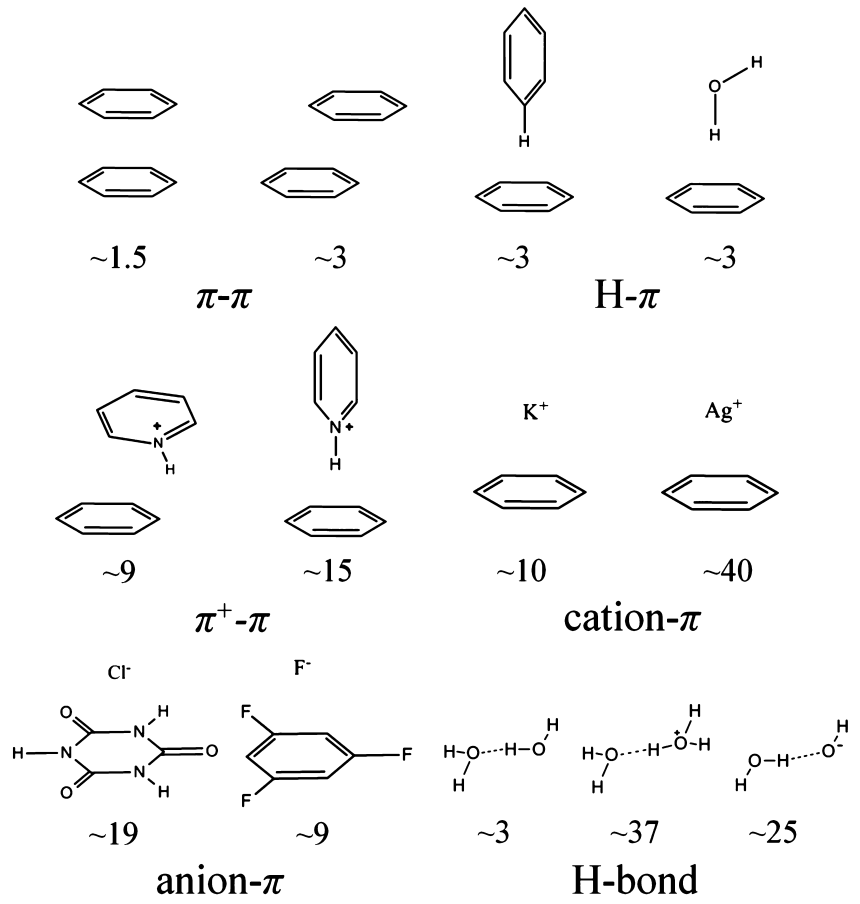

Figure 1. Binding energies (kcal/mol) of various π-interactions ($\pi-\pi$, H$-\pi$, $\pi^+-\pi$, cation$-\pi$, and anion$-\pi$ interactions).[3] The cooperation vs competition of noncovalent interactions govern molecular assembly. Neutral, cationic, and anionic H-bondings[9] are also presented for comparison.

molecular structures, dynamics, and quantum properties.[1,2] There are various types of noncovalent interactions such as ionic interactions, hydrogen bonding, π-interactions, nitrogen bonding, and halogen bonding, which play important roles in chemical, material, and biological systems. Here, we focus our attention on the accuracy of dispersion correction for DFT, in order to properly describe structures and properties of π-systems. Proper choices of density functionals for diverse π-interactions[3] have helped us to design intriguing molecular receptors or sensors, functional molecules and materials, and molecular electronic devices.

π-Interactions can play an important role in applications. Carbon-based systems can often arrange in well-ordered forms due to π-interactions (Figure 1). Compared with H-bonding, the π-interaction has smaller electrostatic energy and increased dispersion energy. In the context of receptor and nanomaterial design, this feature deserves attention because the electrostatic energy contribution is drastically reduced in the presence of high dielectric materials such as polar solvents. Thus, π-interactions play important roles in molecular assembly in solution. Although their magnitudes are small compared with typical reaction energies, the π-interactions can be control elements in chemical reactions.[4−8] They are also vital for good transport properties, because planar π-systems with well-ordered stacked structures are generally conductive.

For understanding structures and properties of π-interaction driven molecular systems, it is essential to perform accurate calculations of larger systems. Although wave function based methods can be more accurate, DFT approaches are inevitable for large systems. However, typical DFT does not include dispersion interactions and so cannot describe π-interactions properly. Several attempts to remedy such an inability of DFT have been made.[10−15] Here, we restrict our attention to schemes correcting the Kohn−Sham energy with estimated dispersion energy.

$$E_{\text{total}} = E_{\text{KS}} + E_{\text{disp}}$$

This dispersion correction adds insignificant costs to the standard DFT calculation and therefore is well-suited for large-scale calculations.

We discuss first the validity of DFT for the interactions in various π-systems. Referring readers to original papers and a recent review,[16] we shortly introduce popular dispersion corrections. Then, we analyze their levels of accuracy and discuss directions for improvements. In the last half of the paper, we present several applications of DFT-D methods with practical implications. Topics include π-molecular recognition, graphene doping, electronic transport on graphene, and magnetic states in layered materials. The balanced description of various interactions is found to be essential in such predictions.

PERFORMANCE OF DISPERSION-CORRECTED DFT METHODS

The goal of the dispersion corrections is to enable DFT to have predictive power for large assemblies of molecules. There are two methods of such corrections; one is pairwise additive

dx.doi.org/10.1021/ar400326q | Acc. Chem. Res. 2014, 47, 3321−3330

correction, and the other is nonlocal correlation. Both have recently shown remarkable success.

First, pairwise additive methods estimate dispersion from all pairs of nuclei:

$$E_{\mathrm{disp}} = -\frac{1}{2}\sum_{\mathrm{A,B}}^{\mathrm{nuc.}}\sum_{n=6,8}\frac{C_{n,\mathrm{AB}}}{R_{\mathrm{AB}}^{\ n}} f_{\mathrm{damp}}(R_{\mathrm{AB}})$$

where R_{AB} is the distance between nuclei A and B, and f_{damp} is the damping function. The R^6 dependence can be easily understood by applying the second-order perturbation theory to two nonoverlapping fragments, considering the interfragment Coulombic interaction as perturbation. Then, the C_6 coefficients are related to the Casimir–Polder integral[17] and represent correlated motion of two instantaneous dipoles. A damping function is used to avoid divergence at short ranges and seamlessly join to the range where conventional density functionals perform well.[18] Popular pairwise-additive corrections are Grimme's D3,[10] Tkatchenko–Scheffler's (TS),[11] and Becke-Johnson's (BJ).[12] D3 uses C_6 obtained from the interpolation of precomputed C_6 according to the "coordination number". TS relies on Hirshfeld partitioning[19] to estimate reduced polarizability in chemical environment. BJ relies on the dispersion driven by exchange-hole dipole moment (XDM). The key achievement of these methods is remarkable transferability of computed dispersion coefficients.

Second, nonlocal correlation methods such as van der Waals density functional (vdW-DF) and its variants have an electron-based formulation, in stark contrast to pairwise additive methods:[13]

$$E_{\mathrm{disp}} = \frac{1}{2}\int\int \mathrm{d}\mathbf{r}\,\mathrm{d}\mathbf{r}'\, n(\mathbf{r})n(\mathbf{r}')\phi(\mathbf{r},\mathbf{r}')$$

where n denotes the electron density and the kernel function ϕ depends on this density and its gradient. Later development of factorization and transform led to widespread use of this approach.[20] This approach in recent implementations gives the electron density self-consistently with nonlocal potential.

Pairwise-additive dispersion corrections can be combined with a variety of density functionals. In the case of nonlocal correlation methods, we have a choice for the exchange enhancement factor. Benchmarks help a user choose a specific combination.[21,22] Still, it is hard to understand why some combinations are better than others. It may not be possible to obtain general and universal functionals unless we know the right reason that some functionals do not work in certain cases. We will discuss the performance of dispersion corrections for π-interactions below.

AROMATIC–π, ALIPHATIC–π, AND NON-π INTERACTIONS

The relative magnitudes of competitive interactions are as important as the absolute magnitude. Wrong ordering will give a wrong guideline toward the design of novel architecture of molecular assembly. For example, competition between aromatic–π interaction and non-π interaction differentiates crystal structures of benzene and cyclohexane. Grimme compared the aromatic–π interactions with aliphatic–π interactions depending on the ring size of aromatic and saturated acenes and addressed the special role of aromatic–π interactions as the size increases.[23] This was further clarified by Sherrill et al.[24] Kim et al. compared aromatic–π, aliphatic–π, and non-π interaction strengths among aromatic π-systems, double or triple-bonded π-systems, and single-bonded aliphatic systems.[25] They reported that various DFT methods gave wrong relative binding strength in aromatic benzene dimer and aliphatic cyclohexane. Here, we expand the results with newly developed dispersion corrections (Figure 2, Table 1). Although these dispersion corrections show much better accuracy, the relative binding strength still has a problem.

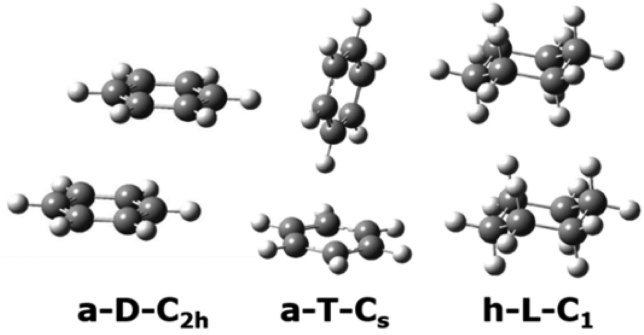

Figure 2. Low energy structures of the benzene (a) dimer and the cyclohexane (h) dimer; (a, aromatic bonded; h, cyclohexane single bonded; D, displaced-stacked; T, T-shaped; L, layered).[25]

The cyclohexane dimer and the benzene dimer (Figure 2) were optimized at the MP2 level followed by the intermolecular distance optimization with CCSD(T) using the aug-cc-pVDZ (aVDZ) basis set. With these geometries, the CBS energies at the CCSD(T) level were estimated.[26] Table 1 shows diverse DFT binding energies of the benzene dimer and the cyclohexane dimer, as well as the CCSD(T)/CBS binding energies as reference. Even recently developed dispersion corrections still give incorrect relative stability between these molecular systems. CCSD(T)/CBS gives the stability in the order of a-T-C_s, a-D-C_{2h}, and h-L-C_1. PBE-TS seems to underestimate polarizability reduction and thus overestimate atomic C_6's and the dispersion energy, as can be noted from a significant improvement from MBD, even though its deviation arises mainly from PBE. Note that the C_6's in D3 for benzene and cyclohexane carbons are 25.4 and 18.3 au, respectively, while those in TS are 31.5 and 30.3 au. On the other hand, the overestimation of D3 for h-L-C_1 is likely due to the $1/R^8$ term, which contributes more to benzene than to cyclohexane. Another reason may be the fact that the polarizability is not isotropic. The C_6 coefficients distinguishing sp^2 and sp^3 carbons assume that the electronic polarizability of a given atom is isotropic, while there does exist a highly anisotropic nature of dispersion that arises from s and $p_x/p_y/p_z$ type orbitals,[27] especially in low-dimensional systems.[28] According to second order perturbation theory, the dispersion energies between two 2s electrons (2s–2s), between two $2p_z$ electrons ($2p_z$–$2p_z$), and between two $2p_1$ electrons ($2p_1$–$2p_1$) for two hydrogenic atoms are quite different.[26] Of course, in molecular systems, anisotropy is much reduced in general, but the orientation difference can still be significant. For example, the anisotropic effect (angular dependence of the size of the atom) in van der Waals radius was described in N_2, O_2, and F_2 (which arises from anisotropic charge driven anisotropic dispersion correction).[29]

To have a deeper insight on dispersion corrections, we investigated the dependence of interaction and dispersion energies on the intermolecular distance of the benzene dimer a-D-C_{2h} (Figure 3). Since not only are π-stacked systems very common in self-assembled structures[30–32] but also dispersion is

dx.doi.org/10.1021/ar400326q | Acc. Chem. Res. 2014, 47, 3321–3330

Table 1. Interaction Energies (kcal/mol) of the Benzene (a) Dimer and the Cyclohexane (h) Dimer

system	CCSD(T)/CBS	B97-D3	PBE + TS	PBE + MBD	vdW-DF	vdW-DF2	opt B88	M06-2X	rPBE + VV10	BLYP-D3[a]	PBE-D3[a]	BLYP + XDM
a-D-C_{2h}	−2.77	−2.57	−3.47	−3.05	−2.98	−2.87	−3.49	−2.53	−3.16	−2.49	−2.51	−2.97
a-T-C_s	−2.91	−3.06	−3.17	−2.90	−2.47	−2.50	−2.93	−2.61	−2.80	−2.42	−2.38	−2.88
h-L-C_1	−2.69	−3.08	−3.85	−3.47	−2.90	−3.05	−3.42	−2.08	−2.78	−2.95	−3.22	−2.90

[a]The TZVPP basis set was used.

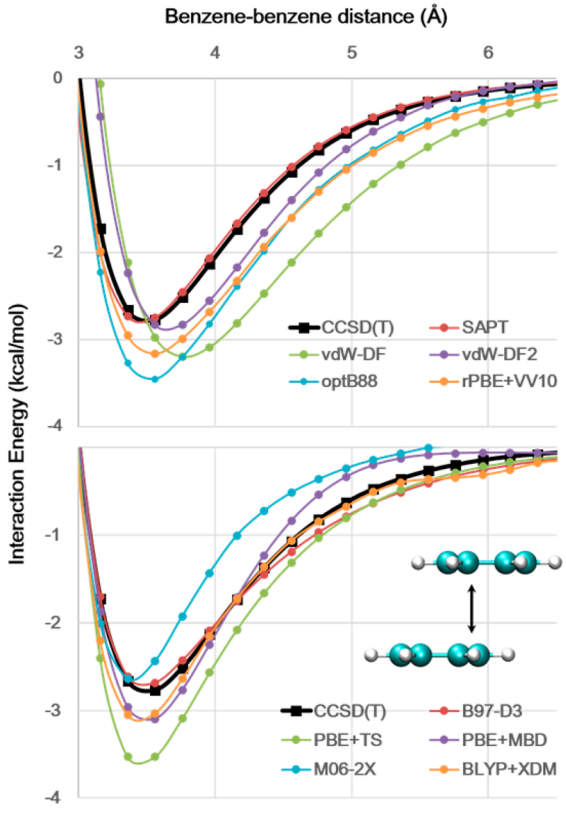

Figure 3. Interaction energy (kcal/mol) of the displaced-parallel structure (a-D-C_{2h}) of the benzene dimer as the benzene−benzene distance (Å) varies.

the most dominant interaction in the displaced-parallel structure of the benzene dimer, we focus on this structure. We define the short-range (shorter than the minimum energy point), midrange (from the minimum energy to the inflection point, ∼1 Å away from the minimum), and long-range (beyond the midrange). The CCSD(T)/CBS interaction energy is considered as the reference. The symmetry adapted perturbation theory (SAPT)[33] values using PBE0AC/aVTZ are very close to the CCSD(T)/CBS curve in the range of interest. Thus, the SAPT dispersion energy can be regarded as a reference for dispersion. B97-D3 agrees very well with the reference, but PBE-D3 slightly overestimates in the midrange. It is thus important to consider which density functional is combined with the dispersion correction. rPBE + VV10 and PBE + TS correctly find the minimum energy distance but overestimate the interaction energy. The overestimation of rPBE + VV10 is almost constant in a large distance range, as also noted in two-dimensional slabs.[34] PBE + MBD[35] (MBD, many-body-dispersion correction) alleviates such an overestimation but diminishes too quickly in the long-range. vdW-DF[12] overestimates both the minimum energy distance and the interaction energy due to the overestimated dispersion. vdW-DF2 (an update from vdW-DF)[36] alleviates both problems. optB88−vdW-DF[37] finds the minimum energy distance correctly but overestimates the dispersion energy. This overestimation can be reduced with the exchange enhancement factor modifying exchange-correlation holes, which define the dielectric function for nonlocal correlations.[38] Although M06-2X is fairly accurate around the minimum, it decays too quickly as the intermolecular distance increases, mainly due to exponential decay of density overlap between monomers. Similar trends were also found for the cytosine−naphthalene interaction.[27]

As discussed above, SAPT provides interaction energies very close to the CCSD(T)/CBS limit for the distances longer than the minimum energy separation. This idea is adopted to develop the dispersionless density functional (dlDF).[39] However, dlDF excludes a part of midrange attractive interaction from the electronic potential and could provide inaccurate results for certain chemical processes (for example, dissociation energies for Cl_3C-Cl, H_3C-Cl, H_3C-CH_3, HO−H, and HO−OH are 10−40 kcal/mol smaller than the experimental values or B3LYP or BLYP values).

Comparing TS and D2 (not shown) with D3 and XDM, one can notice that the pairwise-additive methods are improved by adding the $1/R^8$ term. Note that the difference between the exact interaction energy and the energy predicted by a given DFT functional is not equal to any damped dispersion energy. One reason is that the very Ansatz of DFT-D is approximate, and another is the error of density functional. The dlDF and B97-D are examples of functionals that try to minimize those errors.

POLARIZATION-DRIVEN VAN DER WAALS INTERACTIONS

It is important to investigate whether various dispersion-corrected DFT methods can correctly describe certain environmental perturbations by the presence of other molecules or ions. To compare B97-D3/TZVPP, PBE0-TS/light-3rd tier, vdW-DF2 with CCSD(T)/CBS, and MP2/CBS, we studied a model system of Ar interacting with a polyaromatic hydrocarbon (PAH) radical of $C_{13}H_9$ (1*H*-phenalen-1-yl), as shown in Figure 4. We considered a molecular environmental perturbation by placing a Na^+ or Cl^- ion on the opposite side from the Ar atom with respect to the facial plane of the PAH. We studied the interaction energies of three systems: (i) PAH···Ar, (ii) Na^+···PAH···Ar, and (iii) Cl^-···PAH···Ar with respect to the PAH···Ar distance (r) where Na^+ or Cl^- is located at 3.5 Å away from the PAH (Figure 4a−c).

As to the energy profiles of all three cases, B97-D3 reasonably reproduces the CCSD(T) results, while vdW-DF2 and PBE0-TS seem to slightly deviate from the CCSD(T) results. The B97-D3 intermolecular interaction energy profiles are in most cases in good fit with the CCSD(T) results due to the optimized energy-fitting parameters used in B97-D3. On

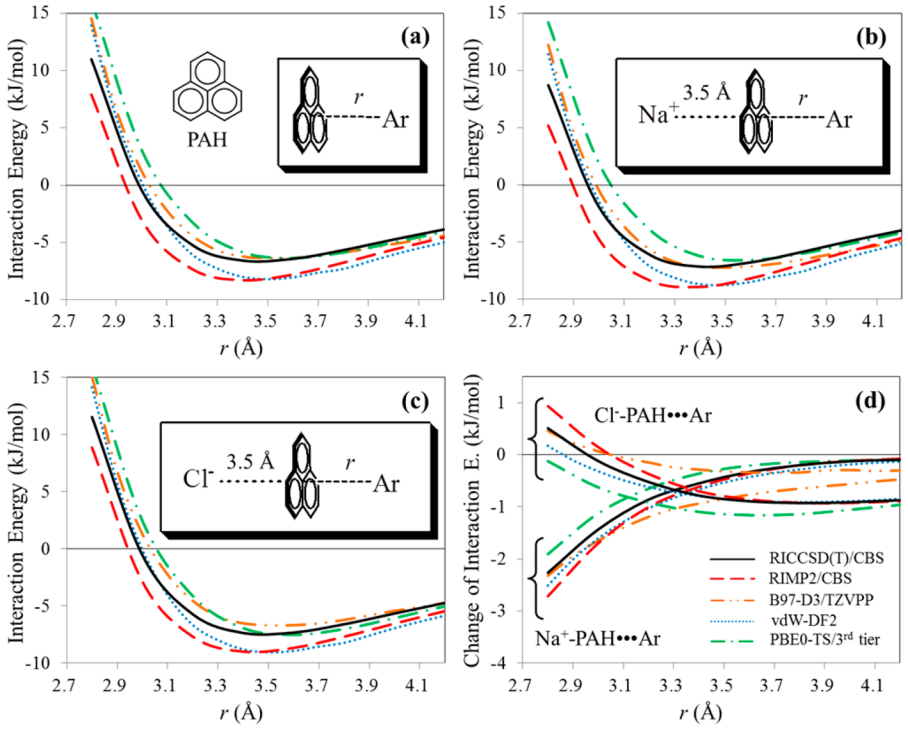

Figure 4. Potential energy curves of (a) PAH···Ar, (b) Na^+···PAH···Ar, and (c) Cl^-···PAH···Ar depending on the PAH−Ar distance for CCSD(T)/CBS, MP2/CBS, vdW-DF2, PBE0-TS/3rd tier, and B97-D3/TZVPP. (d) Change of the interaction energy of Ar with PAH−Na^+ or −Cl^- from that with PAH.

the other hand, the dispersion energies are derived from the converged electron density in the vdW-DF2 and PBE0-TS methods. In such approximations, the interaction energies around the equilibrium point may not be as good as the B97-D3 case where the direct parameter fitting to the accurate interaction energies is performed. Nevertheless, both vdW-DF2 and PBE0-TS seem to properly reproduce the change of dispersion interaction upon the deformation of electron cloud arising from the electric field induced by the neighboring atoms/ions. These are well reflected in energy changes due to the presence of Na^+ or Cl^- in the PAH−Ar system in Figure 4d where vdW-DF2 and PBE0-TS reproduce the CCSD(T) results very well. As such, B97-D3 needs to improve the fitting in consideration of polarization-driven energy changes, while both vdW-DF2 and PBE0-TS need to better describe the absolute interaction energies. One alternative could be to exploit dlDF. However, care is needed in certain cases where dissociation energies are not accurate.

EXTENSION TO LARGE π-SYSTEMS

As discussed above, most small aromatic π-systems can be reasonably described by recently developed dispersion corrections. However, it is questionable whether these corrections are equally accurate for very large systems. Most benchmarks are based on small systems because accurate reference data for large systems are unavailable except for some indirect data sets.[40,41] A challenging aspect in large systems is that an increasing number of interacting atoms collectively generates effects that are negligible in small systems.[28]

Adsorption such as nucleobases on graphene is a good example.[36] These systems are relevant to nanochannel-based DNA sequencing.[42,43] The binding energy of a cytosine to naphthalene is less than half of the binding energy to graphene (Figure 5a). Although the binding configuration is similar, its binding energy on circumcoronene (made up of 54 carbons) is

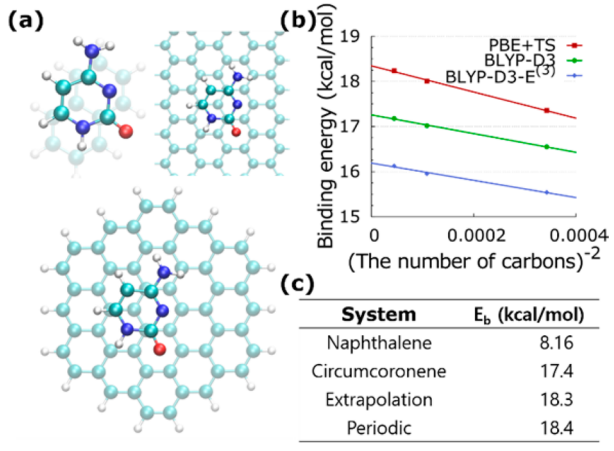

System	E_b (kcal/mol)
Naphthalene	8.16
Circumcoronene	17.4
Extrapolation	18.3
Periodic	18.4

Figure 5. (a) Optimized geometries of a cytosine molecule on PAHs of increasing sizes (H, white; C, green; N, blue; O, red). (b) Increasing binding energy as the number of carbons in the PAH is increased. (c) Comparison of binding energies on PAHs of increasing sizes.[27]

~0.5 kcal/mol weaker than that on graphene. The interaction energy did not converge until the system was increased to a size as large as circumcoronene (Figure 5b). The slight disagreement between periodic and nonperiodic systems comes from the interaction with periodic images and the relaxation of carbons (Figure 5c). Thus, caution is necessary when computing the adsorption energy with dispersion corrections. Moreover, higher-order interactions play a role in large systems in a direction that the binding energy is reduced. Grimme used the binding energies deduced from experiments as the reference

dx.doi.org/10.1021/ar400326q | Acc. Chem. Res. 2014, 47, 3321−3330

and showed that the Axilrod−Teller−Muto type three-body interaction, representing triple-dipole dispersion, alleviates overbinding of pairwise methods.[41] In the case of cytosine on graphene, it reduces the binding energy by 1 kcal/mol (Figure 5b).

We also found that overbinding can be reduced by taking into account dynamic dielectric screening and many-body terms[42] (involving more than two atoms when expanding dispersion as atomic contributions that arise as an approximation of the random-phase-approximated correlation energy). In the buckyball catcher complex (C_{60}@$C_{60}H_{28}$), the $\pi-\pi$ interactions are dominant (Figure 6). A diffusion Monte

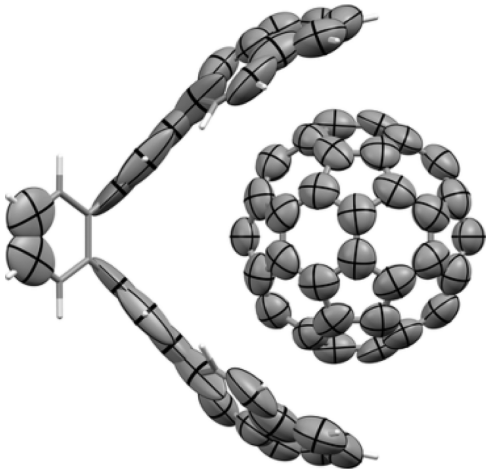

Figure 6. Anisotropy in the atomic polarizabilities of the C_{60}@$C_{60}H_{28}$ complex,[44] where the polarizability tensors are illustrated as ellipsoids.

Carlo (DMC) calculation gives the binding energy of 26 ± 2 kcal/mol. As compared with this value, most DFT methods with pairwise vdW interactions seem to overestimate the stability of this complex by 9−17 kcal/mol possibly because of the lack of dynamical dielectric screening effects, the isotropic treatment of atomic polarizability tensors, and the lack of many-body dispersion terms.

DFT-ASSISTED DESIGN OF FUNCTIONAL MATERIALS AND ELECTRONIC AND SPINTRONIC MOLECULAR DEVICES

We describe a series of applications where DFT prediction of noncovalent π-interactions plays a key role. First, we discuss molecular recognition regarding molecular catchers for fullerene. Noncovalent interactions impart a molecule selectivity and sensitivity, indispensable to sensors. Second, we provide examples from surface physics and electronics and spintronics for graphene and porphyrin involving noncovalent π-interactions.

Molecular Recognition and Sensing

A quintuply charged imidazole-based homocalix compound, calix[5]imidazolium, recognizes neutral fullerenes through $\pi^+-\pi$ interactions and immensely enhances the solubility in water (Figure 7).[45] This could be useful in aqueous fullerene chemistry. In the previous paragraph, we discussed that accurate estimation of dispersion strength is subtle. However, DFT-D3 already gives results consistent with experimental data. B97-D3/TZV2P predicts a binding energy of 21 kcal/mol for the complexation of calix[5]imidazolium·5Br with neutral C_{60}

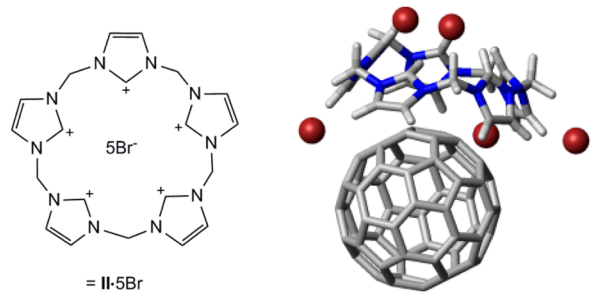

Figure 7. Complexation of calix[5]imidazolium·5Br with neutral C_{60} fullerene.[45]

fullerene in the gas phase. When the implicit solvent effect is included in the gas phase geometry, the binding energy in water is reduced to a half the gas-phase binding energy (10 kcal/mol) due to the presence of the substantial induction energy, which is susceptible to the high dielectric constant of water. Once this geometry is optimized in water using COSMO,[46] the binding energy is slightly increased to 14 kcal/mol.

Extending to Periodic Systems: Material Engineering toward Low Dimensional Electronics

Many layered materials are stabilized by the interlayer interactions of noncovalent type, such as graphite. Thus, it is important to describe the dispersion properly. For example, the interlayer distance of graphite predicted by conventional DFT calculations (∼4.5 Å) is larger than the experimental value (3.35 Å). Sometimes unphysical results of unbound layers are obtained depending on the exchange-correlation functional used. However, with inclusion of the dispersion correction, it gives much better agreement with experiment (∼3.4 Å).[47] For $FeCl_3$-intercalated graphene, the conventional DFT functionals erroneously predicted interlayer distances larger than the experimental value by 0.5−1.0 Å. However, the error in the dispersion-corrected calculation was only ∼0.1 Å.[47] Such an important role of the van der Waals interlayer interaction was also investigated for other layered systems. The self-assembled architecture from the interface between InAs(111) and graphene was explained by van der Waals type interaction, supported by a good agreement with experiment.[48]

Proper inclusion of dispersion interaction is also crucial in describing electronic properties because of the substantial structural changes. In the case of bilayer graphene (BLG), the magnitude of band gap opening is proportional to the potential energy difference between two layers. Such a difference can be achieved by sandwiching BLG between layers of large electronegativity difference, that is, dual-doping.[47] Since the distance between the outermost doping layers affects the potential energy difference of two graphene layers, it is necessary to predict the interlayer distance correctly. Park et al. have optimized the dual-doped BLG system with dispersion correction and obtained consistent description on the experimentally measured transport gap.[49] Furthermore, a correct geometry of BLG dual-doped by $FeCl_3$ and K layers was obtained with dispersion-corrected calculation, and Yang et al. predicted a substantial energy gap with accessible shift of Dirac point.[47] As shown in Figure 8, the doping with $FeCl_3$ (K) alone induces an energy gap of 0.31 (0.43) eV, and the dual-doping opens an energy gap of 0.88 eV. Also, the shift of the Dirac point is as small as 0.09 eV, which is within the range accessible by fabrication techniques. In the case of single layer graphene on SiO_2, the orientation of $CHCl_3$ molecules

dx.doi.org/10.1021/ar400326q | Acc. Chem. Res. 2014, 47, 3321−3330

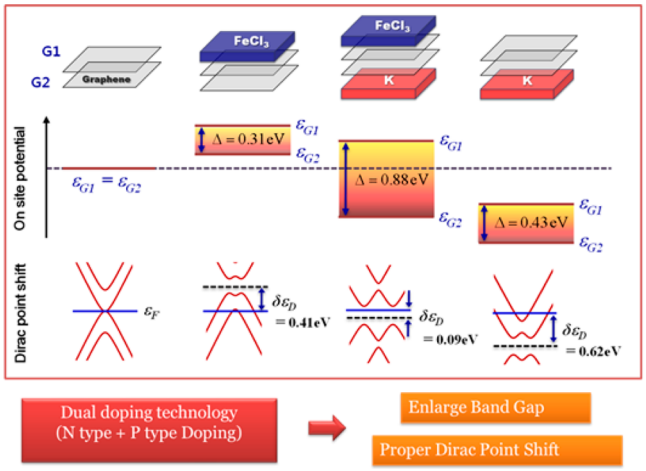

Figure 8. Dual-doping of bilayer graphene by $FeCl_3$ and K layers whose electronegativity values differ largely.[47] vdW-DF is used to describe dispersion (G1/2, upper/lower-graphene; Δ, onsite potential difference; $\delta\varepsilon_D$, Dirac point shift).

intercalated between graphene and SiO_2 was an important factor to explain the observed work function shift. It is because the electric dipole moment of $CHCl_3$ changes the graphene work function depending on the degree of dispersion correction. Kim et al. found a preferable orientation with dispersion correction, and the predicted increase of work function, 0.56 eV, was consistent with the experiment (0.58 eV).[50] All the above agreements between calculations and experiments were based on the correct interaction distances between graphene and dopants. Without proper dispersion correction, the interaction distances are too long, which results in insufficient doping effect.

Implications for Device Modeling: Molecular Spintronic Devices and Quantum Transport

Inspired by the synthesis of fully conjugated one-dimensional zinc porphyrin array (Zn-PA),[51] Cho et al. studied the magnetic properties of PA's containing divalent paramagnetic metal ions at the center (Figure 9a).[52] The porphyrin ligand serves as a strong-field square-planar ligand, which leaves four of the d orbitals nearly degenerate, and destabilizes the one in direct interaction with the nitrogen atoms (Figure 9b). Therefore, the calculated magnetization is maximum for M = Cr, which has four d electrons. However, spontaneous magnetic ordering could not be observed due to the large intermetallic distances. Assuming that the ferromagnetic (FM) ordering can be forced using an external magnetic field, they found that the porphyrin array with Cr^{2+} ion (Cr-PA) shows half-metallic properties, the origin of which can be attributed to the half-filling of the four d orbitals at the bottom. The conduction band of the bare porphyrin array is shown in red in Figure 9c. This band shows spin-splitting in Cr-PA (red and blue lines in Figure 9c), the major spin band above and the minor spin band below the Fermi energy, making the system half-metallic.

The use of this Cr-PA in realistic devices is limited due to the lack of ferromagnetic order. Having recognized the importance of spontaneous magnetic ordering in the design of spintronic devices, we investigated the effect of dispersion correction on the magnetic coupling by comparing the PBE functional with and without TS correction. We designed a system where dispersion interaction can bring the magnetic centers closer, which might lead to a stronger interaction. As a possible

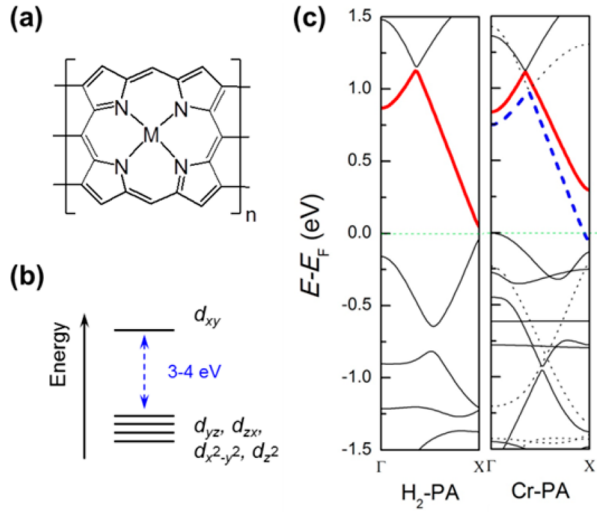

Figure 9. (a) The structure of the porphyrin array with the central metal denoted with M, (b) d orbital splitting pattern inside the porphyrin ligand, and (c) comparison of the band structures of the bare porphyrin array without the metal (H_2-PA) and that with chromium (Cr-PA). The conduction band responsible for the half-metallic property is highlighted with color (solid/dotted line, major/minor spin state).[52]

realization, Mn(III)−porphyrin cation ($MnPP^+$) and cyclopentadienyl anion (Cp^-) can be stacked in an alternating manner (MnPPCp) as multilayered stacking architecture (Figure 10). This design relies on the fact that $MnPP^+$ is

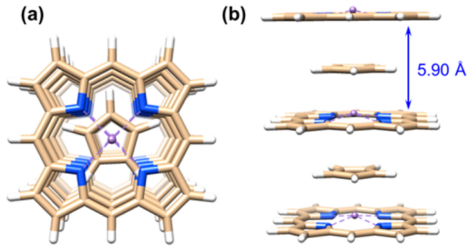

Figure 10. Structure of MnPPCp optimized with PBE + TS method: (a) top and (b) side views.

isoelectronic with Cr(II)-porphyrin and bears a positive charge, so that it can form a one-dimensional structure with the Cp^- anion. The optimized Mn−Mn distance is 5.90 and 6.50 Å with and without the correction, respectively. The shortened distance between the metal centers leads to the change of magnetic coupling. When the TS correction is not used, the FM state is more stable than the antiferromagnetic (AFM) state by 9.4 meV per two Mn units. However, the more compact unit cell resulting from the TS correction reverses this preference, making the AFM state more stable by 4.1 meV. The magnitude of stabilization experienced by FM and AFM states from the dispersion correction is almost the same. As such, the effect of dispersion correction on the prediction of magnetism deserves further study.

Dispersion plays an important role in novel DNA sequencing device using GNR (Figure 11). A nucleobase stacked on GNR blocks ballistic transport at the energy of a molecular orbital. Transmission probability drops by one quantum due to Fano resonance.[53] Since each type of nucleobase has a characteristic eigenvalue spectrum, a DNA strand can be sequenced. The

dx.doi.org/10.1021/ar400326q | Acc. Chem. Res. 2014, 47, 3321−3330

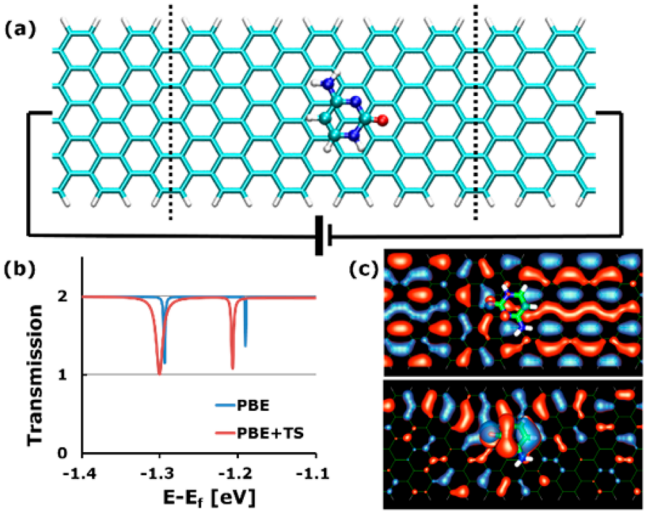

Figure 11. (a) A DNA sequencing device where the currents flow along a GNR. (b) Transmission characteristics when cytosine is adsorbed to GNR. The current drop occurs at the gate voltage characteristic of DNA nucleobases via Fano resonance. The TS dispersion correction brings cytosine close to the GNR so that Fano coupling is increased. (c) The band structure of the system comprised of cytosine and graphene for off/on resonance. The ballistic transport occurs through the continuous electron transfer path in the absence of resonating molecular orbital (upper), whereas the transport is blocked due to the broken electron path due to Fano resonance (lower), which results in the loss of one quantum transport channel, that is, a dip on the transport curve in panel b.[42]

coupling between a nucleobase and GNR determines the experimental measurability of the transmission drop. The dispersion interaction enhances the coupling because it decays exponentially as the adsorption distance is increased. Indeed, PBE expects a negligible coupling since missing dispersion yields too large adsorption distance. PBE + TS enhances the coupling since dispersion brings cytosine closer to the GNR.

■ CONCLUSION

Recently developed dispersion corrections to the Kohn−Sham density functional energy achieved great success. The key to their success lies in the dependence on the chemical environment. To achieve better accuracy in pairwise additive methods, the polarization-driven anisotropic dispersion interaction can be considered, the $1/R^8$ terms representing the dipole−quadrupole interaction can be included, an optimal combination of a dispersion correction with density functional would be used, and for large systems many-body terms could be taken into account. Although many dispersion corrections do not meet all the above conditions, they gave reasonably accurate predictions for applications. In particular, we applied dispersion corrections to molecular recognition, graphene systems, and porphyrin complexes. We note that π-interaction driven recognition, graphene doping, and the magnetic state of metal-porphyrin cannot be correctly predicted without dispersion corrections. The dispersion correction plays an essential role in balanced description of intermolecular interactions.

■ AUTHOR INFORMATION

Corresponding Author

*E-mail address: kimks@unist.ac.kr.

Notes

The authors declare no competing financial interest.
[‖]Y.C. and W.J.C. are co-first-authors.

Biographies

Yeonchoo Cho received his Ph.D. degree from POSTECH. He is a research scientist in Samsung Electronics. His research interests include theoretical methods for molecular electronics/spintronics.

Woo Jong Cho received his Ph.D. degree from POSTECH. He is a postdoctoral fellow in UNIST. His research interests include spintronic materials and water phase-transition.

Il Seung Yoon is a Ph.D. candidate in POSTECH. His research interests include computer-aided molecular design.

Geunsik Lee received his Ph.D. degree from POSTECH. After his postdoctoral experience in University of Texas at Dallas, he was a WCU research assistant professor in POSTECH. He is now an assistant professor in UNIST. His research interests include strongly correlated systems.

N. Jiten Singh received his Ph.D. degree from POSTECH. He is a senior researcher in Samsung SDI. His research interests include supramolecular chemistry and energy materials.

Kwang S. Kim received his Ph.D. degree from University of California, Berkeley. He was a professor in POSTECH. He is a distinguished professor in UNIST. His research interests include nanomaterials and nanodevices.

■ ACKNOWLEDGMENTS

This work was supported by NRF (National Honor Scientist Program, 2010-0020414). We thank the referees for useful comments.

■ REFERENCES

(1) Singh, N. J.; Lee, H. M.; Hwang, I.-C.; Kim, K. S. Designing ionophores and molecular nanotubes based on molecular recognition. *Supramol. Chem.* **2007**, *19*, 321−332.
(2) Riley, K. E.; Pitonak, M.; Jurečka, P.; Hobza, P. Stabilization and structure calculations for noncovalent interactions in extended molecular systems based on wave function and density functional theories. *Chem. Rev.* **2010**, *110*, 5023−5063.
(3) Singh, N. J.; Min, S. K.; Kim, D. Y.; Kim, K. S. Comprehensive energy analysis for various types of π-interaction. *J. Chem. Theory Comput.* **2009**, *5*, 515−529.
(4) Riley, K. E.; Hobza, P. On the importance and origin of aromatic interactions in chemistry and biodisciplines. *Acc. Chem. Res.* **2013**, *46*, 927−936.
(5) Sherrill, C. D. Energy component analysis of π interactions. *Acc. Chem. Res.* **2012**, *46*, 1020−1028.
(6) Krenske, E. H.; Houk, K. N. Aromatic interactions as control elements in stereoselective organic reactions. *Acc. Chem. Res.* **2013**, *46*, 979−989.
(7) Wheeler, S. E. Understanding substituent effects in noncovalent interactions involving aromatic rings. *Acc. Chem. Res.* **2013**, *46*, 1029−1038.
(8) Kim, K. S.; Tarakeshwar, P.; Lee, J. Y. Molecular clusters of π-systems: Theoretical studies of structures, spectra and origin of interaction energies. *Chem. Rev.* **2000**, *100*, 4145−4185.
(9) Pak, C.; Lee, H. M.; Kim, J. C.; Kim, D.; Kim, K. S. Theoretical investigation of normal to strong hydrogen bonds. *Struct. Chem.* **2005**, *16*, 187−202.
(10) Grimme, S.; Antony, J.; Ehrlich, S.; Krieg, H. A consistent and accurate *ab initio* parametrization of density functional dispersion correction (DFT-D) for the 94 elements H-Pu. *J. Chem. Phys.* **2010**, *132*, No. 154104.

(11) Tkatchenko, A.; Scheffler, M. Accurate molecular van der Waals interactions from ground-state electron density and free-atom reference data. *Phys. Rev. Lett.* **2009**, *102*, No. 073005.
(12) Becke, A. D.; Johnson, E. R. Exchange-hole dipole moment and the dispersion interaction revisited. *J. Chem. Phys.* **2007**, *127*, No. 154108.
(13) Dion, M.; Rydberg, H.; Schröder, E.; Langreth, D. C.; Lundqvist, B. I. Van der Waals density functional for general geometries. *Phys. Rev. Lett.* **2004**, *92*, No. 246401.
(14) Zhao, Y.; Truhlar, D. G. The M06 suite of density functionals for main group thermochemistry, thermochemical kinetics, noncovalent interactions, excited states, and transition elements: two new functionals and systematic testing of four M06-class functionals and 12 other functionals. *Theor. Chem. Acc.* **2008**, *120*, 215−241.
(15) Vydrov, O. A.; Van Voorhis, T. Nonlocal van der Waals density functional: The simpler the better. *J. Chem. Phys.* **2010**, *133*, No. 244103.
(16) Klimeš, J.; Michaelides, A. Perspective: Advances and challenges in treating van der Waals dispersion forces in density functional theory. *J. Chem. Phys.* **2012**, *137*, No. 120901.
(17) Casimir, H. B. G.; Polder, D. The influence of retardation on the London-van der Waals Forces. *Phys. Rev.* **1948**, *73*, 360−372.
(18) Grimme, S.; Ehrlich, S.; Goerigk, L. Effect of the damping function in dispersion corrected density functional theory. *J. Comput. Chem.* **2011**, *32*, 1456−1465.
(19) Hirshfeld, F. L. Bonded-atom fragments for describing molecular charge densities. *Theor. Chem. Acc.* **1977**, *44*, 129−138.
(20) Román-Pérez, G.; Soler, J. M. Efficient implementation of a van der Waals density functional: application to double-wall carbon nanotubes. *Phys. Rev. Lett.* **2009**, *103*, No. 096102.
(21) Marom, N.; Tkatchenko, A.; Rossi, M.; Gobre, V. V.; Hod, O.; Scheffler, M.; Kronik, L. Dispersion interactions with density-functional theory: benchmarking semiempirical and interatomic pairwise corrected density functionals. *J. Chem. Theory Comput.* **2011**, *7*, 3944−3951.
(22) Goerigk, L.; Grimme, S. A thorough benchmark of density functional methods for general main group thermochemistry, kinetics, and noncovalent interactions. *Phys. Chem. Chem. Phys.* **2011**, *13*, 6670−6688.
(23) Ehrlich, S.; Moellmann, J.; Grimme, S. Dispersion-corrected density functional theory for aromatic interactions in complex systems. *Acc. Chem. Res.* **2013**, *46*, 916−926.
(24) Hohenstein, E. G.; Sherrill, C. D. Density fitting and Cholesky decomposition approximations in symmetry-adapted perturbation theory: Implementation and application to probe the nature of π-interactions in linear acenes. *J. Chem. Phys.* **2010**, *132*, No. 184111.
(25) Kim, K. S.; Karthikeyan, S.; Singh, N. J. How different are aromatic π interactions from aliphatic π interactions and non-π stacking interactions? *J. Chem. Theory Comput.* **2011**, *7*, 3471−3477.
(26) Min, S. K.; Lee, E. C.; Lee, H. M.; Kim, D. Y.; Kim, D.; Kim, K. S. Complete basis set limit of *ab initio* binding energies and geometrical parameters for various typical types of complexes. *J. Comput. Chem.* **2008**, *29*, 1208−1221.
(27) Cho, Y.; Min, S. K.; Yun, J.; Kim, W. Y.; Tkatchenko, A.; Kim, K. S. Noncovalent interactions of DNA bases with naphthalene and graphene. *J. Chem. Theory Comput.* **2013**, *9*, 2090−2096.
(28) Gobre, V. V.; Tkatchenko, A. Scaling laws for van der Waals interactions in nanostructured materials. *Nat. Commun.* **2013**, *4*, No. 2341.
(29) Kim, H.; Doan, V. D.; Cho, W. J.; Madhav, M. V.; Kim, K. S. Anisotropic charge distribution and anisotropic van der Waals radius leading to intriguing anisotropic noncovalent interactions. *Sci. Rep.* **2014**, *4*, No. 5826.
(30) Stornaiuolo, M.; De Kloe, G. E.; Rucktooa, P.; Fish, A.; van Elk, R.; Edink, E. S.; Bertrand, D.; Smit, A. B.; de Esch, I. J. P.; Sixma, T. K. Assembly of a π-π stack of ligands in the binding site of an acetylcholine-binding protein. *Nat. Commun.* **2013**, *4*, No. 1875.
(31) Lee, J. Y.; Hong, B. H.; Kim, W. Y.; Min, S. K.; Kim, Y.; Jouravlev, M. V.; Bose, R.; Kim, K. S.; Hwang, I.-C.; Kaufman, L. J.; Wong, C. W.; Kim, P.; Kim, K. S. Near-field focusing and magnification through self-assembled nanoscale spherical lenses. *Nature* **2009**, *460*, 498−501.
(32) Georgakilas, V.; Otyepka, M.; Bourlinos, A. B.; Chandra, V.; Kim, N.; Kemp, K. C.; Hobza, P.; Zboril, R.; Kim, K. S. Functionalization of graphene: Covalent and noncovalent approaches, derivatives and applications. *Chem. Rev.* **2012**, *112*, 6156−6214.
(33) Jeziorski, B.; Moszynski, R.; Szalewicz, K. Perturbation theory approach to intermolecular potential energy surfaces of van der Waals complexes. *Chem. Rev.* **1994**, *94*, 1887−1930.
(34) Björkman, T.; Gulans, A.; Krasheninnikov, A. V.; Nieminen, R. M. van der Waals bonding in layered compounds from advanced density-functional first-principles calculations. *Phys. Rev. Lett.* **2012**, *108*, No. 235502.
(35) Tkatchenko, A.; DiStasio, R. A.; Car, R.; Scheffler, M. Accurate and efficient method for many-body van der Waals interactions. *Phys. Rev. Lett.* **2012**, *108*, No. 236402.
(36) Lee, K.; Murray, E. D.; Kong, L.; Lundqvist, B. I.; Langreth, D. C. Higher-accuracy van der Waals density functional. *Phys. Rev. B* **2010**, *82*, No. 081101.
(37) Klimes, J.; Bowler, D. R.; Michaelides, A. Chemical accuracy for the van der Waals density functional. *J. Phys.: Condens. Matter* **2010**, *22*, No. 022201.
(38) Hyldgaard, P.; Berland, K.; Schröder, E. Interpretation of van der Waals density functionals. *Phys. Rev. B* **2014**, *90*, No. 075148.
(39) Pernal, K.; Podeszwa, R.; Patkowski, K.; Szalewicz, K. Dispersionless density functional theory. *Phys. Rev. Lett.* **2009**, *103*, No. 263201.
(40) Risthaus, T.; Grimme, S. Benchmarking of London dispersion-accounting density functional theory methods on very large molecular complexes. *J. Chem. Theory Comput.* **2013**, *9*, 1580−1591.
(41) Grimme, S. Supramolecular binding thermodynamics by dispersion-corrected density functional theory. *Chem.—Eur. J.* **2012**, *18*, 9955−9964.
(42) Min, S. K.; Kim, W. Y.; Cho, Y.; Kim, K. S. Fast DNA sequencing with a graphene-based nanochannel device. *Nat. Nanotechnol.* **2011**, *6*, 162−165.
(43) Rajan, A. C.; Rezapour, M. R.; Yun, J.; Cho, Y.; Cho, W. J.; Min, S. K.; Lee, G.; Kim, K. S. Two dimensional molecular electronics spectroscopy for molecular fingerprinting, DNA sequencing and cancerous DNA recognition. *ACS Nano* **2014**, *8*, 1827−1833.
(44) Tkatchenko, A.; Alfè, D.; Kim, K. S. First-principles modeling of non-covalent interactions in supramolecular systems: the role of many-body effects. *J. Chem. Theory Comput.* **2012**, *8*, 4317−4322.
(45) Chun, Y.; Singh, N. J.; Hwang, I.-C.; Lee, J. W.; Yu, S. U.; Kim, K. S. Calix[n]imidazolium as a new class of positively charged homocalix compounds. *Nat. Commun.* **2013**, *4*, No. 1797.
(46) Klamt, A.; Schüürmann, G. COSMO: A new approach to dielectric screening in solvents with explicit expressions for the screening energy and its gradient. *J. Chem. Soc., Perkin Trans. 2* **1993**, *5*, 799−805.
(47) Yang, J. W.; Lee, G.; Kim, J. S.; Kim, K. S. Gap opening of graphene by dual $FeCl_3$-acceptor and K-donor doping. *J. Phys. Chem. Lett.* **2011**, *2*, 2577−2581.
(48) Hong, Y. J.; Yang, J. W.; Lee, W. H.; Ruoff, R. S.; Kim, K. S.; Fukui, T. Van der Waals epitaxial double heterostructure: InAs/single-layer graphene/InAs. *Adv. Mater.* **2013**, *25*, 6847−6853.
(49) Park, J.; Jo, S. B.; Yu, Y.-J.; Kim, Y.; Yang, J. W.; Lee, W. H.; Kim, H. H.; Hong, B. H.; Kim, P.; Cho, K.; Kim, K. S. Single-gate bandgap opening of bilayer graphene by dual molecular doping. *Adv. Mater.* **2012**, *24*, 407−411.
(50) Kim, H. H.; Yang, J. W.; Jo, S. B.; Kang, B.; Lee, S. K.; Bong, H.; Lee, G.; Kim, K. S.; Cho, K. Substrate-induced solvent intercalation for stable graphene doping. *ACS Nano* **2013**, *7*, 1155−1162.
(51) Tsuda, A.; Osuka, A. Fully conjugated porphyrin tapes with electronic absorption bands that reach into infrared. *Science* **2001**, *293*, 79−82.

(52) Cho, W. J.; Cho, Y.; Min, S. K.; Kim, W. Y.; Kim, K. S. Chromium porphyrin arrays as spintronic devices. *J. Am. Chem. Soc.* **2011**, *133*, 9364−9369.
(53) Cho, Y.; Min, S. K.; Kim, W. Y.; Kim, K. S. The origin of dips for the graphene-based DNA sequencing device. *Phys. Chem. Chem. Phys.* **2011**, *13*, 14293−14296.